Pergamon

Int. J. Heat Mass Transfer. Vol. 39, No. 11, pp. 2243–2252, 1996

0017-9310/96 $15.00 + 0.00

0010-9310(95)00334-7

Inclined and horizontal wall plumes

H.-T. LIN, J.-J. CHEN, L.-W. KUNG and W.-S. YU
Chemical Engineering Department, National Central University, Chungli, Taiwan 320, Republic of China

and

Y.-M. CHEN
Mechanical Engineering Department, National Taiwan University, Taipei, Taiwan 106, Republic of China

(*Received in final form* 23 *August* 1995)

Abstract—This work studied, both theoretically and experimentally, the inclined wall plumes which arise from a line thermal source imbedded at the leading edge of an adiabatic plate with arbitrary tilt angle between 0 and $\pi/2$. An appropriate formulation and a very effective numerical scheme are developed to obtain rigorous numerical solutions over the full range of tilt angle from the horizontal to the vertical for fluids of any Prandtl number between 0.001 and 1000. The effects of the tilt angle on the velocity and temperature profiles are presented. A simple, but very accurate, correlation equation is proposed for predicting the wall temperature of the inclined plate over the whole range of tilt angle for $0.001 \leqslant Pr \leqslant 1000$.

The temperature fields of air over the inclined plates have been visualized by using holographic interferometry. The photographs of interferograms confirm the physical reality of the horizontal and the inclined wall plumes. Copyright © 1996 Elsevier Science Ltd.

1. INTRODUCTION

In an analysis of buoyancy induced laminar flows adjacent to horizontal surfaces with power-law variations of wall temperature, i.e. $T_w - T_\infty = Nx^n$, Blanc and Gebhart [1] obtained similarity boundary-layer equations with the exponent constant n limited by $-1/2 \leqslant n \leqslant 2$ for physical reality. The case of the lower limit of $n = -1/2$ is equivalent to a buoyant wall plume along an adiabatic horizontal plate. In a similarity analysis of mixed convection flow over a horizontal plate, Schneider [2] has mentioned a particular case of no heat transfer at the wall except in the singular point at the leading edge. It is indeed the case of a horizontal wall plume. This kind of plume has rarely been investigated. On the other hand, a vertical wall plume arising from a line thermal source imbedded at the leading edge of an adiabatic vertical plate has been studied extensively [3–11].

In most practical situations the plate is usually inclined rather than exactly vertical or horizontal. However, in contrast to the extensive experimental and theoretical investigations on free convection heat transfer from heated inclined plates, there seems to be no prior analysis on a buoyancy-induced wall plume along an adiabatic inclined plate. This has motivated the present study.

In this paper, we analyze the inclined wall plumes adjacent to an adiabatic plate with tilt angle between 0 and $\pi/2$. By introducing proper dimensionless variables, we are able to obtain a set of nonsimilar equations which provides very accurate solutions for arbitrary plate inclination from the horizontal to the vertical and for fluids of any Prandtl number between 0.001 and 1000. Moreover, the nonsimilar equations are readily reducible to the self-similar equations of the vertical and the horizontal wall plumes.

To solve the set of nonsimilar plume equations subject to an integral constraint equation of flux-conservation condition, we develop a very effective numerical scheme. The proposed numerical procedure can be applied to the analyses of other plumes.

Usually, one would expect a plume rises upward from a line heat source rather than develops along the surface of a horizontal plate as a boundary-layer flow. However, the presence of a semi-infinite plate restricts the entrainment flow on one side of the plume. Consequently, the plume would lie on the plate surface by the buoyancy-induced longitudinal pressure gradient. In order to convince one of the physical reality of a horizontal wall plume and the inclined wall plumes of large tilt angle, we carried out an experiment to visualize the horizontal and the inclined wall plumes by using holographic interferometry.

2. ANALYSIS

In this study we consider a buoyancy-induced wall plume along an inclined adiabatic plate, which arises from a line heat source imbedded at the leading edge of the plate. The physical model and coordinate sys-

NOMENCLATURE

c	constant
c_p	specific heat [J kg^{-1} K^{-1}]
f	dimensionless stream function, $\Psi/\alpha\zeta$
g	gravitational acceleration [m s^{-2}]
k	thermal conductivity [J s^{-1} m^{-1} K^{-1}]
K	Gladstone–Dale constant [m^3 kg^{-1}]
L	length of line thermal source [m]
m	constant
M	molecular weight [kg mol^{-1}]
n	constant
N	numbers of the bright fringes of interferograms
p	dynamic pressure [N m^{-2}]
P	atmospheric pressure [atm]
Pr	Prandtl number, ν/α
Q	rate of heat released from the line source [J s^{-1}]
R	ideal gas constant [atm m^3 mol^{-1} K^{-1}]
Ra	Rayleigh number, $gT^*x^3/\alpha\nu$
T	fluid temperature [K]
T_w	wall temperature [K]
T_∞	temperature of ambient fluid [K]
T^*	equivalent temperature of the line source, $Q/(\rho c_p \alpha L)$ [K]
u	velocity component in the x-direction [m s^{-1}]
v	velocity component in the y-direction [m s^{-1}]
x	coordinate along the plate [m]
y	coordinate normal to the plate [m].

Greek symbols

α	thermal diffusivity, $k/\rho c_p$ [m^2 s^{-1}]
β	thermal expansion coefficient [K^{-1}]
ζ	$(\sigma Ra\cos\varphi)^{1/5}+(\sigma Ra\sin\varphi)^{1/6}$
η	pseudo-similarity variable, $(y/x)\zeta$
θ	dimensionless temperature, $(T-T_\infty)\zeta/T^*$
λ	wavelength [m]
μ	dynamic viscosity [kg m^{-1} s^{-1}]
ν	kinematic viscosity [m^2 s^{-1}]
ξ	$[1+(\sigma Ra\sin\varphi)^{1/6}/(\sigma Ra\cos\varphi)^{1/5}]^{-1}$
ρ	density of fluid [kg m^{-3}]
σ	$Pr/(1+Pr)$
τ_w	wall shear stress, $\mu(\partial u/\partial y)_{y=0}$ [kg m^{-1} s^{-2}]
φ	tilt angle measured from the vertical [degree]
Ψ	stream function [m^2 s^{-1}].

Subscripts

i	ith iteration
w	at the wall
∞	far from the wall.

tem are shown in Fig. 1. The flat plate is inclined with an arbitrary tilt angle φ to the vertical from 0 to $\pi/2$, including the vertical and the horizontal orientations. On the basis of boundary-layer and Boussinesq approximations, the governing equations of the inclined wall plume can be written as

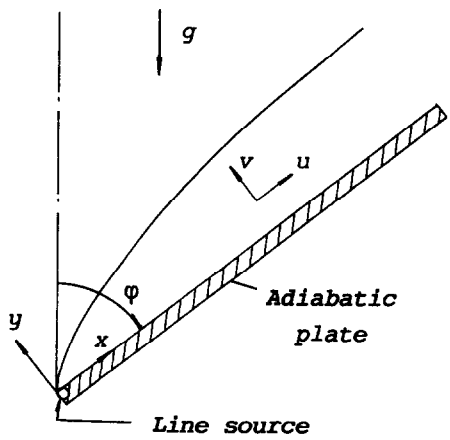

Fig. 1. Physical model and coordinate system.

$$\frac{\partial u}{\partial x}+\frac{\partial v}{\partial y}=0 \tag{1}$$

$$u\frac{\partial u}{\partial x}+v\frac{\partial u}{\partial y}=-\frac{1}{\rho}\frac{\partial p}{\partial x}+\nu\frac{\partial^2 u}{\partial y^2}+g\beta(T-T_\infty)\cos\varphi \tag{2}$$

$$0=-\frac{1}{\rho}\frac{\partial p}{\partial y}+g\beta(T-T_\infty)\sin\varphi \tag{3}$$

$$u\frac{\partial T}{\partial x}+v\frac{\partial T}{\partial y}=\alpha\frac{\partial^2 T}{\partial y^2}. \tag{4}$$

The boundary conditions are

$$u=0,\quad v=0,\quad \partial T/\partial y=0\quad \text{at } y=0; \tag{5}$$

and

$$u=0,\quad p=0,\quad T=T_\infty\quad \text{as } y\to\infty. \tag{6}$$

In addition to the boundary conditions, the governing equations are also subject to a constraint of energy conservation. That is, the total energy convected by the boundary-layer flow through the per-

pendicular plane at any $x > 0$ must be equal to the energy Q released from the line thermal source:

$$\rho c_p L \int_0^\infty u(T-T_\infty)\,dy = Q. \tag{7}$$

To facilitate the analysis of the wall plume on a plate with arbitrary inclination from the vertical to the horizontal, we propose a dimensionless group

$$\xi = \left[1+\frac{(\sigma Ra\sin\varphi)^{1/6}}{(\sigma Ra\cos\varphi)^{1/5}}\right]^{-1} \tag{8}$$

where

$$\sigma = Pr/(1+Pr) \tag{9}$$

and the local Rayleigh number Ra is defined as

$$Ra = g\beta T^* x^3/\alpha\nu \tag{10}$$

with the equivalent temperature T^* given by

$$T^* = Q/(\rho c_p \alpha L). \tag{11}$$

The variable ξ describes the relative strength of the longitudinal to the transverse components of buoyant force acting on the boundary-layer flow adjacent to the inclined plate. It is also a parameter that represents the degree of inclination. For the limiting case of a vertical plate, $\varphi = 0$, consequently, $\xi = 1$. While for the other limiting case of a horizontal plate, $\varphi = \pi/2$, and thus $\xi = 0$. The dimensionless variable ξ can also be regarded as a stretched longitudinal coordinate.

In addition, a pseudo-similarity variable is defined as

$$\eta = (y/x)\zeta \tag{12}$$

where

$$\begin{aligned}\zeta &= (\sigma Ra\cos\varphi)^{1/5} + (\sigma Ra\sin\varphi)^{1/6}\\ &= (\sigma Ra\cos\varphi)^{1/5}/\xi\\ &= (\sigma Ra\sin\varphi)^{1/6}/(1-\xi).\end{aligned} \tag{13}$$

Furthermore, a dimensionless stream function, a dimensionless dynamic pressure, and a dimensionless temperature are defined, respectively, as follows:

$$f(\xi,\eta) = \psi(x,y)/\alpha\zeta \tag{14}$$

$$\omega(\xi,\eta) = (px^2/\rho\alpha^2)/\zeta^4 \tag{15}$$

$$\theta(\xi,\eta) = [(T-T_\infty)/T^*]\zeta \tag{16}$$

where $\psi(x,y)$ is the stream function that satisfies the continuity equation (1).

By substituting the independent variables ξ, η and the dimensionless dependent variables f, ω and θ into equations (1)–(7), we obtain

$$\begin{aligned}&Prf''' + \frac{5+\xi}{10}ff'' - \frac{\xi}{5}f'f'\\ &\quad + \frac{5-\xi}{10}\eta\omega' - \tfrac{2}{5}\xi\omega + (1+Pr)\xi^5\theta\\ &\quad = \tfrac{1}{10}\xi(1-\xi)\left[f'\frac{\partial f'}{\partial\xi} - f''\frac{\partial f}{\partial\xi} + \frac{\partial\omega}{\partial\xi}\right]\end{aligned} \tag{17}$$

$$\omega' = (1+Pr)(1-\xi)^6\theta \tag{18}$$

$$\theta'' + \frac{5+\xi}{10}(f\theta)' = \tfrac{1}{10}\xi(1-\xi)\left[f'\frac{\partial\theta}{\partial\xi} - \theta'\frac{\partial f}{\partial\xi}\right] \tag{19}$$

$$f(\xi,0) = 0, \quad f'(\xi,0) = 0, \quad \theta'(\xi,0) = 0 \tag{20}$$

$$f'(\xi,\infty) = 0, \quad \omega(\xi,\infty) = 0, \quad \theta(\xi,\infty) = 0 \tag{21}$$

and

$$\int_0^\infty f'\theta\,d\eta = 1 \tag{22}$$

where the primes denote differentiation with respect to η.

For the limiting case of a horizontal wall plume, $\xi = 0$, equations (17)–(19) are readily reduced to the following self-similar equations:

$$Prf''' + \tfrac{1}{2}ff'' + \tfrac{1}{2}(1+Pr)\eta\theta = 0 \tag{23}$$

$$\theta'' + \tfrac{1}{2}(f\theta)' = 0 \tag{24}$$

while for the other limiting case of a vertical wall plume, $\xi = 1$ and $\omega = 0$. Therefore, equations (17)–(19) become

$$Prf''' + \tfrac{3}{5}ff'' - \tfrac{1}{5}f'f' + (1+Pr)\theta = 0 \tag{25}$$

$$\theta'' + \tfrac{3}{5}(f\theta)' = 0. \tag{26}$$

3. NUMERICAL METHOD

In this section, an effective finite-difference procedure is developed to solve the nonsimilar equations (17)–(19) of the inclined wall plume with boundary conditions (20) and (21) subject to an integral equation (22) of energy flux conservation. This integral equation of constraint makes a feature of the plume system. However, it is very difficult to integrate the set of system equations constrained by this integral equation, especially when the system equations are nonsimilar. One of the valuable contributions of this work is to introduce a finite-difference procedure for solving effectively the nonsimilar plume equations subject to such an integral equation. This numerical procedure is a modified version of Keller's Box method which has been well described in ref. [12]. The essential modification is that an additional iteration scheme was joined to the Keller's numerical procedure to certify that the integral equation is satisfied at each ξ_n.

As the first step of the numerical procedure, equations (17)–(19) are rewritten as a system of first-order equations which are then discreted by using central

difference equations. There results a set of nonlinear difference equations for the unknowns at ξ_n in terms of their values at ξ_{n-1}. Next, these nonlinear difference equations were linearized by Newton's method. Finally, the linearized equations and the appropriate boundary conditions are written in matrix–vector form and solved by the Keller's block-elimination method [12].

If equations (20) and (21) were used as boundary conditions, infinite numbers of solutions would be obtained. But only one of these solutions can satisfy the integral constraint equation (22). Therefore, we developed an iteration scheme to search for the unique solution that simultaneously satisfies equations (20), (21) and the integral equation (22). To incorporate the integral equation, we drop the boundary condition $\theta'(\xi, 0) = 0$ and replace it with a presupposed boundary condition.

$$\theta(\xi, 0) = H \tag{27}$$

where H is a guessed constant. The linearized difference equations, along with the corresponding expressions for the boundary conditions (20), (21) and (27), can be solved conveniently and efficiently by using the block-elimination method to give a converged solution at ξ_n. The obtained converged solution has to satisfy the constraints of equations (20) and (22). If not, an iteration algorithm

$$H_{i+1} = H_i - \frac{\theta_i'(\eta = 0)\dfrac{\partial \theta_i'(\eta = 0)}{\partial H} + (I_i - 1)\dfrac{\partial I_i}{\partial H}}{\left(\dfrac{\partial \theta_i'(\eta = 0)}{\partial H}\right)^2 + \left(\dfrac{\partial I_i}{\partial H}\right)^2} \tag{28}$$

is carried out to predict a new value of H for the next trial until the following criterion is satisfied:

$$[\theta_i'(\xi, 0)]^2 + (I_i - 1)^2 < 10^{-8} \tag{29}$$

where the subscript i denotes the ith iteration, and

$$I_i = \int_0^\infty f_i' \theta_i \, d\eta. \tag{30}$$

The derivatives $\partial \theta_i'(\eta = 0)/\partial H$ and $\partial I_i/\partial H$ for the calculations of the iteration equation (28) are obtained by solving a system of linear difference equations known as the variational equations [12]. The variational equations are derived by taking the derivatives of the difference equations and their boundary conditions with respect to H. These equations can also be efficiently solved by the Block-elimination method to give all the derivatives that are required for the computation of $\partial \theta_i'(\eta = 0)/\partial H$ and $\partial I_i/\partial H$.

Once the unique converged solution at ξ_n has been obtained, which satisfies all the boundary conditions and the integral equation of constraint, the numerical procedure is repeated for ξ_{n+1}. This solution process is marched forward step-by-step from $\xi = 0$ to $\xi = 1$ with uniform step size of $\Delta\xi = 0.01$. The solution along $\xi = 0$ is required to initiate the numerical procedure. This solution can be obtained from the numerical integration of the similar equations (23) and (24) subject to the boundary conditions of equations (20), (21) and the integral equation (22), by using the Runge–Kutta scheme in connection with the shooting technique.

The step size of $\Delta\eta$ and the edge of the boundary layer η_∞ were varied from $\Delta\eta = 0.02$ and $\eta_\infty = 15$ for small values of Pr to $\Delta\eta = 0.1$ and $\eta_\infty = 60$ for large values of Pr.

4. EXPERIMENTAL SETUP AND TEST SECTION

A schematic of the test section (side view) is shown in Fig. 2. The test section is basically a flat plate of Bakelite (350 mm × 170 mm × 4 mm). A Nichrome wire of diameter 1 mm and length 170 mm was imbedded at the leading edge of the plate as a line heat source, which has been connected to a d.c. power supply.

In this experiment, a double exposure holographic interferometry [13, 14] was employed. The schematic diagram of the optical setup for holographic interferometry is shown in Fig. 3. A 20 mW He–Ne laser of 632.8 nm wavelength was used as the coherent and monochromatic light source. The interferograms were recorded on an Agfa-8E75 holographic plate. Details of holographic interferometry have been well described in the literature [13, 14] and will not be repeated here.

5. NUMERICAL RESULTS AND DISCUSSIONS

5.1. *Velocity profiles*

The longitudinal component of velocity is related to $f'(\xi, \eta)$ by the following equation

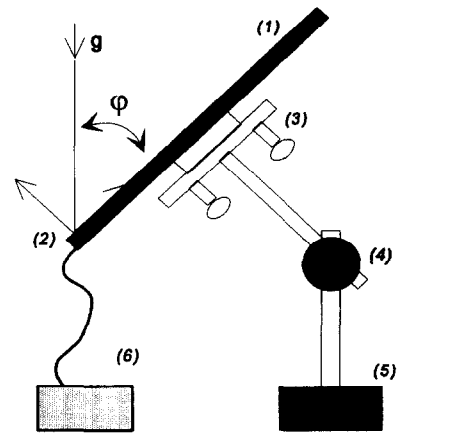

Fig. 2. Schematic of the test section of an inclined plate with a line heat source at the leading edge.

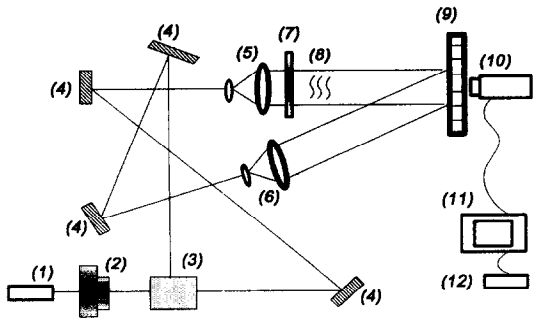

Fig. 3. Schematic diagram of the experimental apparatus.

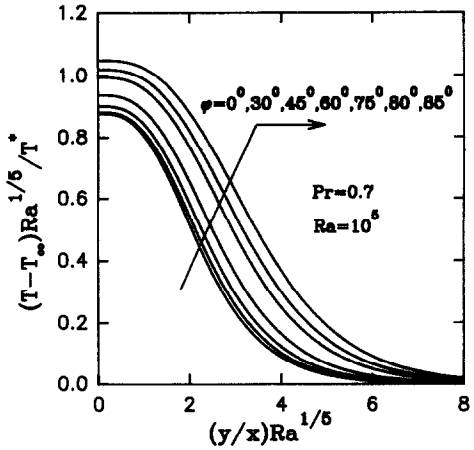

Fig. 5. Representative temperature profiles, $Pr = 0.7$, $Ra = 10^5$.

$$u(x,y) = (\alpha/x)\xi^2 f'(\xi,\eta). \tag{31}$$

This equation can be rewritten as

$$\frac{u}{\alpha/x} = \frac{(\sigma Ra\cos\varphi)^{2/5}}{\xi^2} f'(\xi,\eta). \tag{32}$$

Typical profiles of the dimensionless velocity $u/(\alpha/x)$ over the dimensionless transverse coordinate (y/x) $Ra^{1/5} = \eta\xi/(\sigma\cos\varphi)^{1/5}$ for some specified tilt angles are shown in Fig. 4 for $Pr = 0.7$ and $Ra = 10^5$. It is shown that the longitudinal velocity decreases when the plate is tilted away from the vertical. This is due to the decrease of the component of buoyancy force with increasing tilt angle measured from the vertical.

5.2. *Temperature profiles*

Representative profiles of the dimensionless temperature

$$\frac{T-T_\infty}{T^*} Ra^{1/5} = \frac{\xi\theta(\xi,\eta)}{(\sigma\cos\varphi)^{1/5}} \tag{33}$$

over the dimensionless transverse coordinate $(y/x)Ra^{1/5}$ are presented in Fig. 5 for $Pr = 0.7$ and $Ra = 10^5$. This figure indicates clearly that the plume temperature increases as the tilt angle from the vertical increases due to a decrease of flow velocity.

5.3. *Wall temperature and friction*

The variations of the dimensionless wall temperature $\theta(\xi,0)$ with ξ for fluids of Prandtl number from 0.001 to 1000 are presented in Fig. 6. To show clearly the variations of wall temperature with the longitudinal position and tilt angle, this figure has been recast as Fig. 7 for a typical case of a line heat source of $Q = 2.42$ J s^{-1}, $L = 17$ cm in air for which all the physical properties are evaluated at the film temperature about 40°C. As expected, the wall temperature decreases with increasing longitudinal distance. This figure also reveals that the wall temperature (the plume temperature as well) decreased due to a more vigorous flow when the plate was tilted away from the horizontal.

The effects of Prandtl number on the dimensionless wall temperature $\theta(\xi,0)$ and the dimensionless wall shear stress $f''(\xi,0) = \tau_w[(\rho\alpha\nu/x^2)\lambda^3]^{-1}$ are illustrated in Fig. 8 for $\xi = 0.5$ as a representative case. The

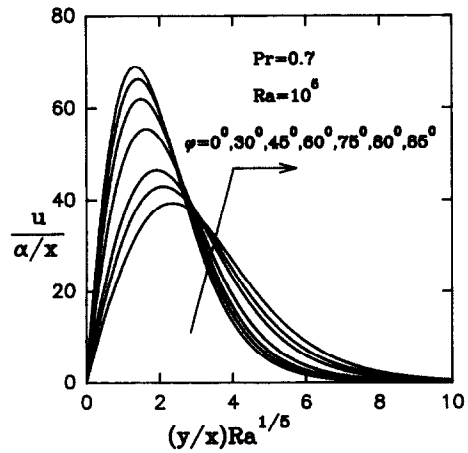

Fig. 4. Representative velocity profiles, $Pr = 0.7$, $Ra = 10^5$.

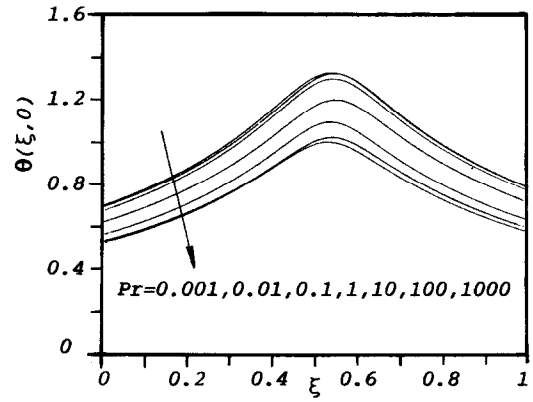

Fig. 6. Variations of the dimensionless wall temperature $\theta(\xi,0)$ with ξ.

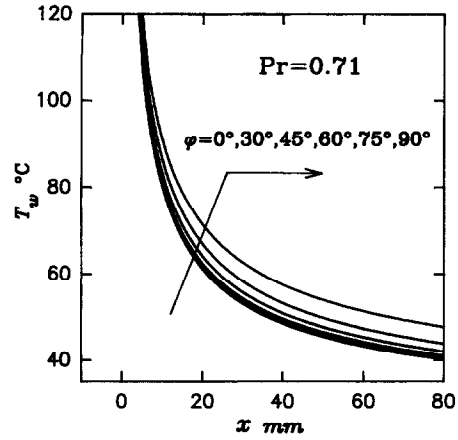

Fig. 7. Variations of the wall temperature with the longitudinal distance and tilt angle.

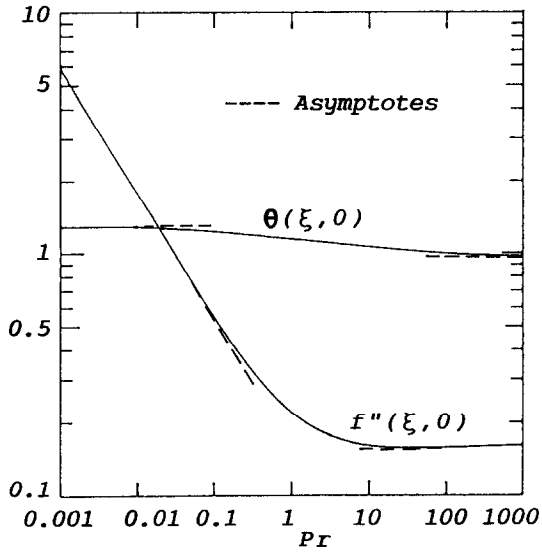

Fig. 8. Variations of $\theta(\xi,0)$ and $f''(\xi,0)$ with Prandtl number, $\xi = 0.5$.

dimensionless wall temperature $\theta(\xi,0)$ decreases slightly with increasing the Prandtl number over the range of $0.001 \leqslant Pr \leqslant 1000$, whereas the wall shear stress decreases linearly with increasing Prandtl number from $Pr = 0.001$ to 10. It approaches to the asymptotic value of $Pr \to \infty$ as $Pr > 10$.

5.4. *Comparison with literature*

Since no previous work on the inclined wall plume is available, a direct comparison is not possible. However, the accuracy of the numerical solutions can be verified by comparing the present results of $\xi = 1$ with reported data of vertical wall plume. For the limiting case of $\xi = 1$, the dimensionless wall temperature $\theta(\xi,0)$ reduces to

$$\theta(1,0) = \frac{T_w - T_\infty}{T^*}(\sigma Ra)^{1/5} \tag{34}$$

and the wall friction can be expressed non-dimensionally as

$$\frac{\tau_w}{(\rho\alpha v/x^2)Ra^{3/5}} = \sigma^{3/5} f''(\xi,0). \tag{35}$$

Table 1. Comparison of the dimensionless wall temperature $[(T_w - T_\infty)/T^*]Ra^{1/5}$ and wall friction $\tau_w[(\rho\alpha v/x^2)Ra^{3/5}]^{-1}$ for the vertical wall plume ($\xi = 1$)

	$[(T_w - T_\infty)/T^*]Ra^{1/5}$		$\tau_w[(\rho\alpha v/x^2)Ra^{3/5}]^{-1}$	
Pr	Present	Ref. [4]†	Present	Ref. [4]†
0.001	3.1589	—	0.8207	—
0.01	1.9934	1.9936	0.9775	0.9779
0.1	1.2599	1.2600	1.0761	1.0763
0.7	0.8771	0.8771	1.0899	1.0900
1	0.8287	0.8340	1.0898	1.0950
7	0.6710	—	1.1109	—
10	0.6546	0.6547	1.1174	0.8796
100	0.6041	0.6038	1.1535	1.1542
1000	0.5888	—	1.1690	—

† Liburdy and Faeth (1975) [4].

The values of the dimensionless wall temperature $[(T_w - T_\infty)/T^*]Ra^{1/5}$ and those of the dimensionless wall friction $\tau_w[(\rho\alpha v/x^2)Ra^{3/5}]^{-1}$ calculated from the numerical data of $\xi = 1$ are compared in Table 1 with the converted data of Liburdy and Faeth [4]. It is seen that the agreement between the two solutions is excellent. Since the set of nonsimilar equations for the inclined wall plume is integrated numerically step-by-step from $\xi = 0$ to $\xi = 1$, the accurate results of $\xi = 1$ ensure that the finite-difference solution are uniformly valid over the entire range of the plate inclination from the horizontal limit to the vertical limit.

5.5. *Correlations of wall temperature*

For convenience of application, we propose a simple correlation equation of dimensionless wall temperature as follows:

$$\left[\frac{1}{\theta(\xi,0)}\right]^m = \left[\frac{1-\xi}{\theta(0,0)}\right]^m + \left[\frac{\xi}{\theta(1,0)}\right]^m. \tag{36}$$

The wall temperature of a vertical wall plume, $\theta(1,0)$, has been correlated [15] for any Prandtl number between 0.001 and infinity as

$$\theta(0) = \theta_\infty(0)\left[\frac{\left(\frac{\theta_0(0)}{\theta_\infty(0)}\right)^c + Pr}{1+Pr}\right]^{1/c} \tag{37}$$

where $\theta_0(0)$ and $\theta_\infty(0)$ represent the values of $\theta(0)$ for $Pr \to 0$ and $Pr \to \infty$, respectively. With

$\theta_0(0) = 0.7933$, $\theta_\infty(0) = 0.5874$ and $c = 5$, the maximum error of equation (37) is less than 3.5% when compared with the numerical data over the range of $0.001 \leqslant Pr \leqslant \infty$.

The same form of correlation can be applied to predict the wall temperature of the horizontal wall plume, $\theta(0,0)$, for any Pr. In this case, we choose $\theta_0(0) = 0.6999$ ($Pr = 0.001$), $\theta_\infty(0) = 0.5268$ ($Pr = 1000$) and $c = 6$. The deviation of this correlation from the numerical results does not exceed 2.8% for $0.001 \leqslant Pr \leqslant 1000$.

We substitute the correlations of $\theta(0,0)$ and $\theta(1,0)$ into equation (36) to fit an appropriate value of exponent constant m by comparing with the numerical results of $\theta(\xi, 0)$. With $m = 6$, the correlation equation has an error less than 4.1% over the entire range of plate inclination for $0.001 \leqslant Pr \leqslant 1000$.

6. EXPERIMENTAL RESULTS AND DISCUSSIONS

The interference images of air temperature field of the inclined wall plumes for some specified tilt angles are shown in Fig. 9. Intuitively, one would expect a

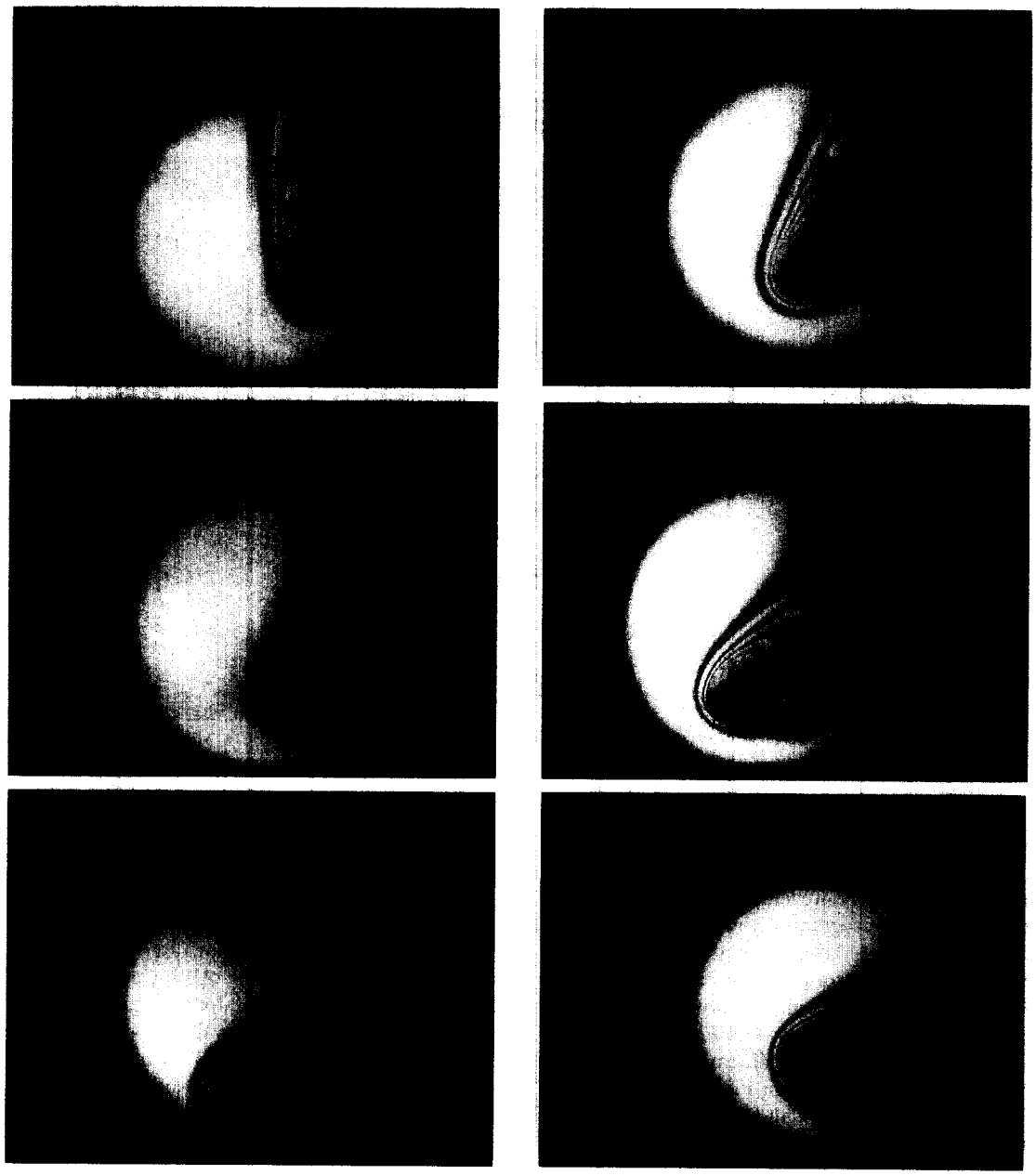

Fig. 9. Photographs of interferograms of the inclined wall plumes: (a) $\varphi = 0°$ (vertical); (b) $\varphi = 30°$; (c) $\varphi = 45°$; (d) $\varphi = 60°$; (e) $\varphi = 75°$ and (f) $\varphi = 90°$ (horizontal).

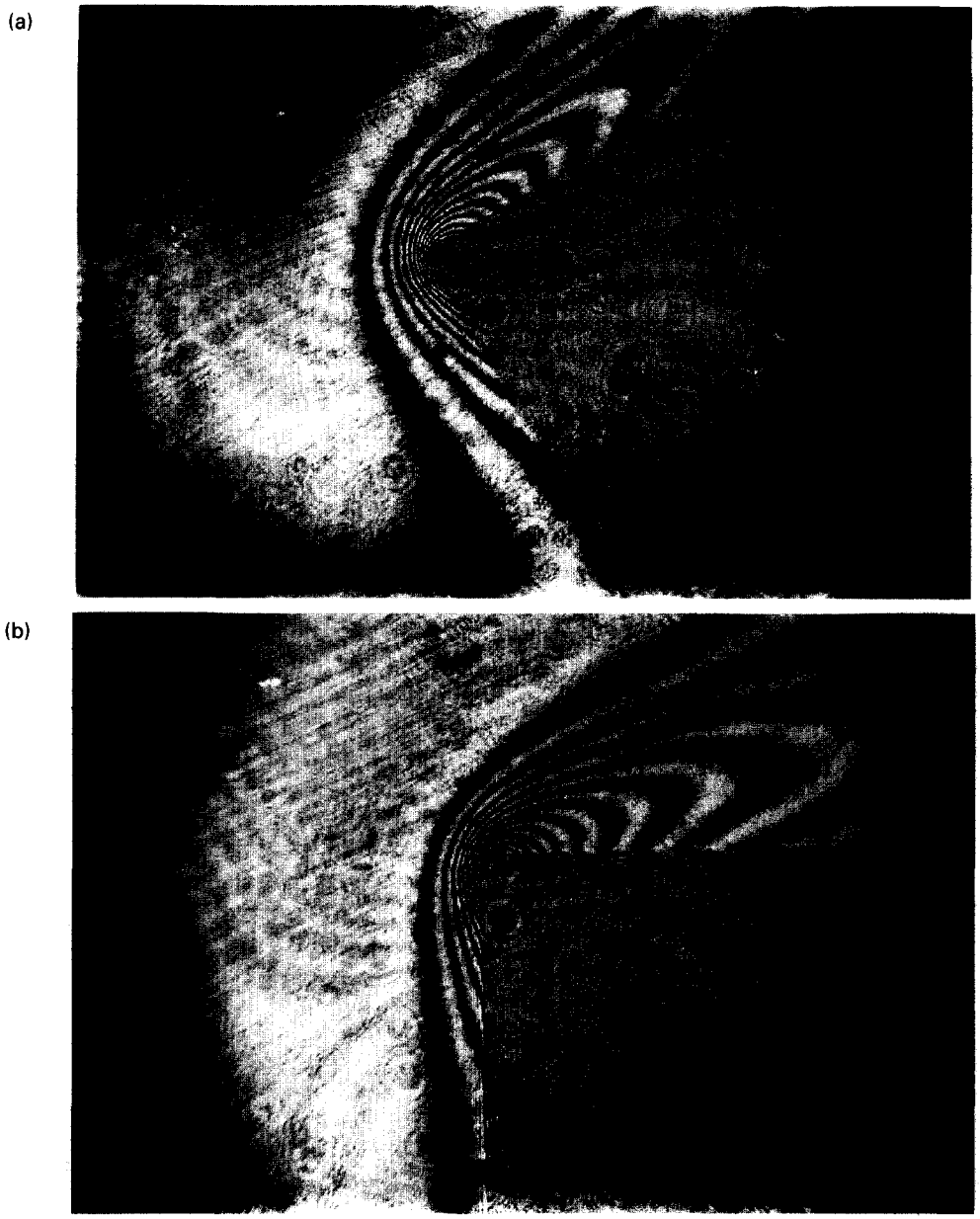

Fig. 10. Photographs of interferograms of the inclined wall plumes adjacent to a block with a line heat source at the edge: (a) $\varphi = 60°$; (b) $\varphi = 90°$.

heat line source induces a vertical plume rather than a boundary layer flow adjacent to the inclined and horizontal plates. However, these photographs of holographic interferograms definitely show that there are stable boundary-layer flows along the plate. No separation and wake formation have been found. The plumes not only develop along a horizontal plate but also along a block, as is shown in Fig. 10.

Experimental results of wall temperature are compared with numerical data in Fig. 11 for the case of $\varphi = 30°$. The theoretical wall temperatures have been calculated from equation (33), while the experimental temperatures were estimated from the fringe pattern of holographic interferograms presented in Fig. 9 by using the following equation modified from ref. [14]:

$$T = \left[\frac{1}{T_\infty} + N\frac{\lambda}{L}\frac{\mathrm{R}}{KPM}\right]^{-1} \tag{38}$$

where N is the number of bright fringes in the interferograms; λ the wavelength of laser light; and K the Gladstone–Dale constant. All the constants and physical properties required for the calculation of theoretical and experimental wall temperatures have been listed in Table 2. Figure 11 clearly shows that the experimental and theoretical results have the same tendency of wall temperature decay. As expected, the wall temperatures estimated from holographic interferometry are lower than the numerical solution due to the heat losses. In the theoretical analysis, we assume that all the thermal energy released from the

Table 2. Experiment conditions, some constants and physical properties used in this study

Experiment conditions:	
Ambient temperature, T_∞	23°C
Pressure, P	1 atm
Wavelength of laser light, λ	632.8×10^{-9} m
Length of the line source, L	1.7×10^{-1} m
Energy rate of the source, Q	2.42 J s^{-1}
Constants:	
Gravitational acceleration, g	9.8 m s^{-2}
Gladstone–Dale constant, K	2.256×10^{-4} m^3 kg^{-1}
Ideal gas constant, R	82.05×10^{-6} atm m^3 mol^{-1} K^{-1}
Molecular weight of air, M	28.8×10^{-3} kg mol^{-1}
Physical properties (at 40°C):	
Thermal diffusivity, α	24.8×10^{-6} m^2 s^{-1}
Thermal expansion coefficient, β	3.19×10^{-3} K^{-1}
Dynamic viscosity, ν	19.123×10^{-6} m^2 s^{-1}
Density, ρ	1.092 kg m^{-3}
Heat capacity, c_p	1.014×10^3 J kg^{-1} K^{-1}
Prandtl number, Pr	0.71
Range of local Rayleigh number:	10^6–10^8

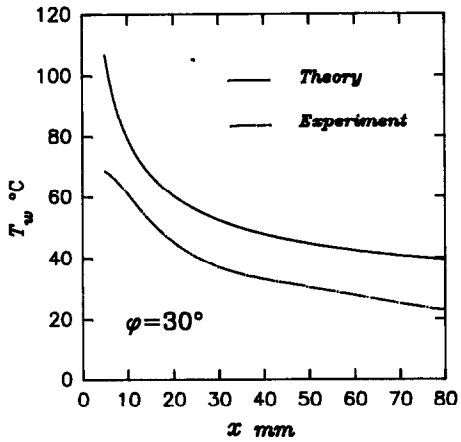

Fig. 11. Comparison of the theoretical and experimental results of wall temperature, $\varphi = 30°$.

line source has been transferred totally to the boundary-layer flow. However, the downward curvature of the isotherms near the wall has revealed that heat flux from the fluid flow to the plate is considerable. Moreover, the interferograms also indicate that there are significant heat transfers to the fluid around the line source due to the large temperature difference between the line source and the ambient fluid.

7. CONCLUSIONS

In this paper, we have analyzed the inclined wall plumes along an adiabatic plate of arbitrary inclination. The following conclusions have been obtained:

(1) By defining properly the dimensionless independent variables, we were able to obtain a set of nonsimilar equations which provides very accurate solutions for any tilt angle from the horizontal to the vertical over a very wide range of Prandtl number.

(2) To solve the set of nonsimilar plume equations subject to an integral equation of flux conservation condition, we have developed a very effective numerical scheme. The proposed numerical procedure can be applied to the analyses of other plumes.

(3) A simple, but very accurate, correlation equation of wall temperature have been developed for a plate with arbitrary inclination and for $0.001 \leqslant Pr \leqslant 1000$.

(4) The plume velocity increases, and the plume temperature decreases consequently, as the tilt angle away from the horizontal increases.

(5) The holographic interferograms do confirm the physical reality of the horizontal and the inclined wall plumes.

Acknowledgements—The authors would like to express their thanks to Professor M.-W. Chang of the Optical Sciences Center, National Central University for his permission to use the laboratory facilities. The support of this work by the National Science council through grant NSC76-0402-E008-04 is gratefully acknowledged.

REFERENCES

1. P. Blanc and B. Gebhart, Buoyancy induced flows adjacent to horizontal surfaces, *Proceedings of the Fifth International Heat Transfer Conference*, Vol. 3, pp. 20–24 (1974).
2. W. Schneider, A similarity solution for combined force and free convection flow over a horizontal plate, *Int. J. Heat Mass Transfer* **22**, 1401–1406 (1979).
3. D. Zimin and Y. N. Lyakhov, Convective wall plume, *J. Appl. Mech. Tech. Phys.* **11**, 159–161 (1970).
4. J. A. Liburdy and G. M. Faeth, Theory of a steady laminar thermal plume along a vertical adiabatic wall, *Lett. Heat Mass Transfer* **2**, 407–418 (1975).
5. Y. Jaluria and B. Gebhart, Buoyancy induced flow arising from a line thermal source on an adiabatic vertical surface, *Int. J. Heat Mass Transfer* **20**, 153–157 (1977).
6. V. P. Carey and J. C. Mollendorf, The temperature field above a concentrated heat source on a vertical adiabatic surface, *Int. J. Heat Mass Transfer* **20**, 1059–1067 (1977).
7. E. M. Sparrow, S. V. Patankar and R. M. Abdul-Wahed,

Development of wall and free plumes above a heated vertical plate, *J. Heat Transfer* **100,** 184–190 (1978).
8. N. Afzal, Convective wall plume: higher order analysis, *Int. J. Heat Mass Transfer* **23,** 505–513 (1980).
9. Y. Jaluria, Mixed convection in a wall plume, presented at the *20th Joint ASME/AIChE National Heat Transfer Conference*, Milwaukee, Wisconsin, 2–5 August, 81-HT-37 (1981).
10. K. V. Rao, B. F. Armaly and T. S. Chen, Analysis of laminar mixed convective plumes along vertical adiabatic surfaces, *J. Heat Transfer* **106,** 552–557 (1984).
11. R. Krixhnamurthy and B. Gebhart, Mixed convection in wall plumes, *Int. J. Heat Mass Transfer* **27,** 1679–1689 (1984).
12. T. Cebeci and P. Bradshaw, *Physical and Computational Aspects of Convective Heat Transfer*. Springer, Berlin (1984).
13. W. Hauf and U. Grigull, Optical methods in heat transfer, *Adv. Heat Transfer* **6,** 133–366 (1970).
14. C. M. Vest, *Holographic Interferometry*. Wiley, New York (1979).
15. H.-T. Lin and W.-T. Cheng, Comprehensive correlations for laminar mixed convection line plume and wall plume, *Int. J. Heat Mass Transfer* **35,** 2751–2753 (1992).